Published in Photonics Technology Letters (IEEE) 12, issue 3, 263-265, 2000
which should be used for any reference to this work

A Quantum Cascade Laser Based on an n-i-p-i Superlattice

Jérôme Faist, *Member, IEEE*, Antoine Müller, Mattias Beck, Daniel Hofstetter, Stephane Blaser, Ursula Oesterle, and Marc Ilegems

***Abstract*—We demonstrate a quantum cascade laser with a novel injection concept. Periodic insertion of silicon- and beryllium-doped layers are used to control locally the internal electric field in the active region. This concept is demonstrated experimentally using an active region based on a periodic superlattice.**

***Index Terms*—Intersubband, lasers.**

QUANTUM cascade (QC) lasers based on intersubband transitions [1] have now demonstrated very high level of performances in the mid-infrared [2]–[8]. Virtually all the high performance [2]–[5] devices operate under an almost homogenous applied electric field. QC lasers based on doped superlattices or with superlattice with a doping inducing a transfer of charge in the injector, however, are notable exceptions [6], [7]. The latter devices do not operate with the same level of performance than the one based on a chirped superlattice under an homogenous applied electric field [8].

The application of an electric field is obviously a necessity in a quantum cascade device. It would be advantageous, however, if a means of canceling or at least decreasing the electric field *locally* inside the active region could be found. For active regions based on localized states [1]–[3] (such as found in the so-called two or three wells active region structures), a reduction of the applied field would increase the confinement of the upper laser state by decreasing its tunneling amplitude into the continuum. This advantage should be more strongly felt in short wavelength QC structures [5].

The situation if even more dramatic for QC lasers with an active region based on extended states such as superlattice active regions. Shown in Fig. 1 is the plot of the product of the interminiband oscillator strength with the upper state lifetime (a figure of merit number which is inversely proportional to the threshold current density for a Quantum Cascade laser) versus electric field for a finite superlattice consisting of five periods of 5.9-nm-thick InGaAs wells and 0.9-nm-thick AlInAs barriers. As it is apparent from the data of Fig. 1, even a small electric field reduces significantly the figure of merit of the superlattice. A reduction of the local applied electric field in these devices is therefore a necessity. It will allow wavefunctions with a large spatial extension, increasing the oscillator strength beyond what is achievable with a chirped superlattice [8]. The extent of these wavefunctions is limited by the available conduction band discontinuity and the oscillator strength is reduced by nonparabolicity.

In previous work, this control of the electric field was obtained either by a homogenous doping of the active region [6] or by a transfer of electrons in the active region [7]. Both techniques only partially control the electric field. Their main disadvantages are that the screening of the electric field is anyway imperfect, tends to decrease with increasing temperature, and require free electron population inside the active region that will induce additional free carrier losses.

In this work, we propose that the electric field inside the active region can be reduced through the use of a plane of p-dopant intercalated between the regular n-dopants sheets of the injection region, as shown schematically in Fig. 2. The basic idea is that in presence of an excess donor density (requiring that the donor density N_d is larger than the acceptor one N_a), the electrons will be transferred to the acceptors until complete saturation of the latter, creating a change in the internal electric field by the amount F_d given by

$$F_d = \frac{N_a q_0}{\epsilon \epsilon_0}$$

where q_0 is the electron charge, ϵ_0 the vacuum dielectric constant and ϵ the relative dielectric constant of the semiconductor. This internal field F_d created by the displacement of the electrons from the donors to the acceptors is used to reduce the electric field in the active region. This technique provides two main advantages. First, because wide bandgap semiconductors are used, i.e., $E_g \gg kT$ the electric field profile is not temperature dependent up to room temperature and above. The other advantage is that the additional charge used to create the additional internal electric field are frozen on their acceptor site and do not participate to the free carrier absorption.

The structure, grown by molecular beam epitaxy on an n-doped InP substrate, consisted of a 25 period active region embedded in an optical waveguide. As shown in Fig. 2 each period of the active region of our sample consists of a six period superlattice with 5.9-nm InGaAs wells and 0.9-nm AlInAs barriers separated by an injection/relaxation region having at each end the Si and Be doping. Early experiments with this concept have shown that it was necessary to insert an undoped spacer layer between the doped region and the active region to minimize dopant diffusion inside the latter [9].

J. Faist, A. Müller, M. Beck, D. Hofstetter, and S. Blaser are with the University of Neuchâtel, CH-2000 Neuchâtel, Switzerland (e-mail: jerome.faist@iph.unine.ch).

U. Oesterle and M. Ilegems are with the Swiss Institute of Technology, CH-1015 Lausanne, Switzerland.

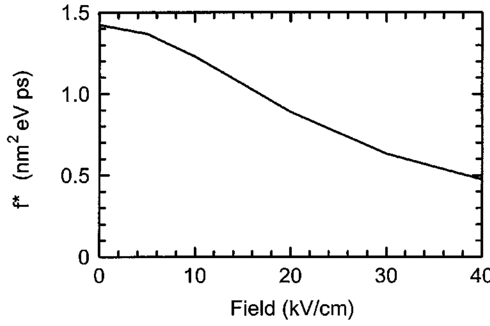

Fig. 1. Product of the oscillator strength and upper state lifetime as a function of applied electric field for a five period 5.9-nm InGaAs wells, 0.9-nm AlInAs barriers superlattice.

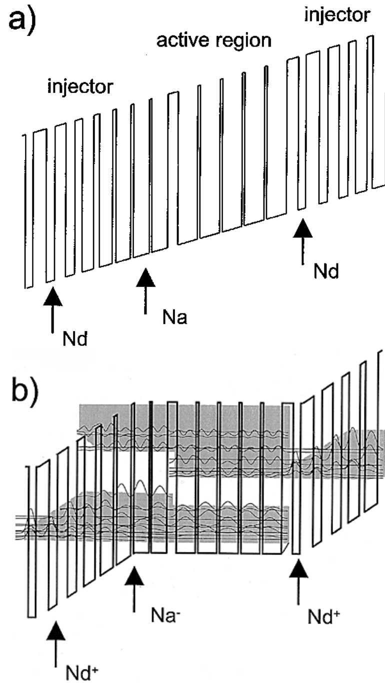

Fig. 2. Schematic band structure explaining the operating principle of the NIPI doping. (a) Schematic conduction band diagram of one stage of the structure under an applied electric field of 2.8×10^4 V/cm in an hypothetical situation where the dopants would not have transferred from the donors levels to the acceptors. (b) Schematic band structure after the electrons have been transferred. The moduli squared of the relevant wavefunctions are shown and their effective occupation in the energy-space diagram is indicated by a grayed area. The layer sequence of one period of structure, in nanometers, left to right and starting from the injection barrier is $2.3/\underline{\mathbf{4.0}/2.6/\mathbf{3.3}/2.7}/\mathbf{2.2}/3.4/\mathbf{1.7}/3.9/\mathbf{1.0}/4.4/\underline{\mathbf{0.9}/4.8}/\mathbf{0.7}/4.8/\mathbf{3.0}/5.9/\mathbf{0.8}/5.9/\mathbf{0.8}/5.9/\mathbf{0.8}/5.9/\mathbf{0.8}/5.9/\mathbf{3.5}/$ where $In_{0.52}Al_{0.48}As$ layers are in bold, $In_{0.53}Ga_{0.47}As$ in roman, numbers underlined with a solid line correspond to doped layer with Si to $N_d = 8 \times 10^{17}$ cm^{-3}, number underlined with dots correspond to layers doped with Be to $N_a = 8 \times 10^{17}$ cm^{-3}. The dopant distribution has been approximated by a delta function in the calculations.

The concept of the charge transfer between the Si and Be dopants is illustrated in Fig. 2(b) where the calculated moduli square of the relevant wavefunctions are displayed along with the band-edge energy. Layer thickness and doping levels are given in the caption of Fig. 2. The optical waveguide is similar to the one of previous QC devices and consists of the InP substrate on one side and of AlInAs cladding layer on the other.

In a finite superlattice, transitions between states with the same parity are forbidden by symmetry at zero electric field. By measuring the intensity of such a forbidden transition as a function of applied voltage, we measure the effective electric field in the superlattice and are therefore able to investigate the effect of the Be doping on the effective internal field. This measurement was performed in devices processed into circular mesas of 200 μm diameter. The superlattice active region of the test sample (S1551) was slightly different from that in Fig. 2, with 5.6-nm-thick wells and 1.3-nm-thick barriers, translating into a narrower lower miniband (with a width of about 85 meV) and a larger minigap (of about 140 meV). The electroluminescence spectra measured as a function of applied bias at $T = 85$ K, are shown in Fig. 3. The three spectral features at 140, 159, and 184 meV are easily identified to the $n = 6$ to $n = 5$ $(6 \rightarrow 5)$, $6 \rightarrow 4$ and $7 \rightarrow 4$ transitions of the five quantum-well active region. The calculated transition energies are 136, 156 and 186 meV. Transition $6 \rightarrow 5$ corresponds to the fundamental gap of the miniband and is the laser transition in superlattice QC lasers. Transition $7 \rightarrow 4$ arises from injection of hot electrons into level 7. Finally, transition $6 \rightarrow 4$ arises when the electric field penetrates into the superlattice. The decrease of the luminescence intensity of the $6 \rightarrow 4$ transition with increasing applied voltage can only be explained by the decrease of its matrix element as the effective field is *decreased* in the active region. In this sample, the minimum field arises at an applied bias of

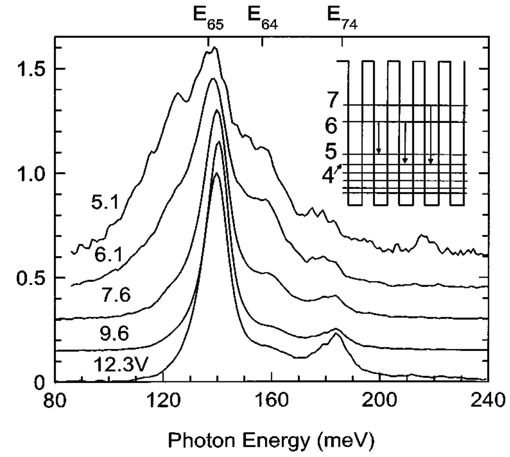

Fig. 3. Luminescence spectra as a function of applied voltage. The calculated transition energies are shown on the upper horizontal axis. The decrease of the $6 \rightarrow 4$ transition as a function of increasing applied bias shows that the internal field decreases, proving the effect of the p-dopant planes.

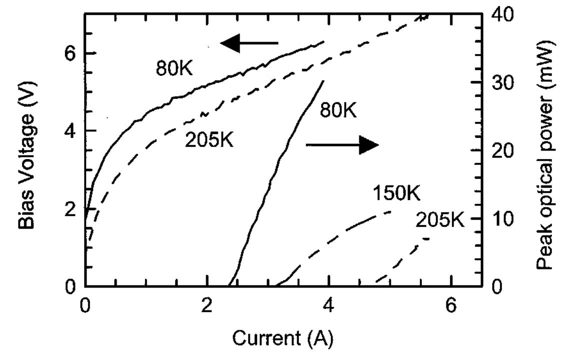

Fig. 4. Bias voltage and optical power as a function of injected current measured in pulsed operation.

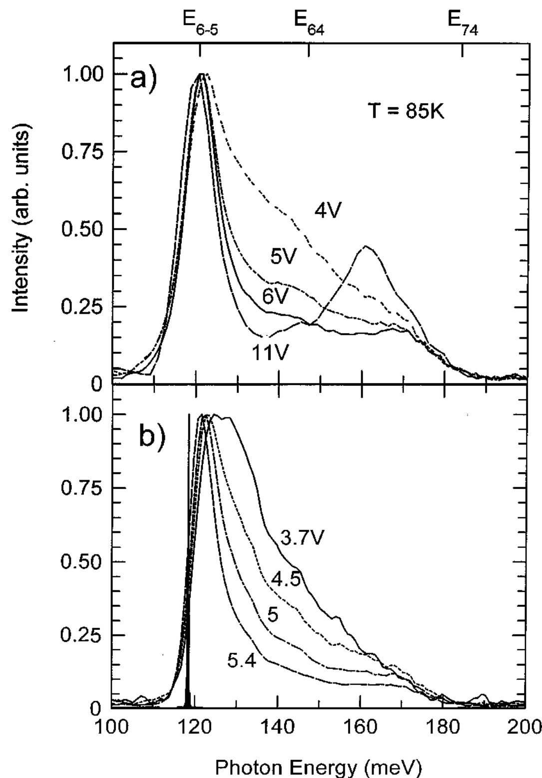

Fig. 5. Electroluminescence spectra as a function of applied voltage for sample S1629. (a) LED device. (b) Laser device.

about 9.6 V. This decrease is uneqvivocal evidence for the action of the Be doping planes. At the maximum voltage (12.6 V), the effective electric field in the active region increases again, as demonstrated by the rise of the $6 \rightarrow 4$ transition. In addition electron heating, which causes injection in state 7, is demonstrated by the rise of the $7 \rightarrow 4$ transition strength. The voltage (~9.6 V) at which the flat band situation was reached in the superlattice was higher than the designed value (6 V), because of a Be doping level larger than intended.

The laser samples (S-1629) were processed into mesa etched ridge waveguides of width 28 μm by wet etching through the active region, ZnSe passivation and Ti–Au metallization. The devices were driven by 50-ns current pulses with a 4.5-kHz repetition rate. Fig. 4 shows the optical power versus drive current from a 1.5-mm-long device for various temperatures between 85 K and 210 K. These curves show clear indication of laser operation with tens of miliwatts of output power. As shown in Fig. 4, the operating voltage is quite low since the laser starts to operate at a voltage of 5.5 V. The threshold current density at 85 K is 6 kA/cm^2 and the laser stop operating at 220 K. The threshold current density increases with temperature with the usual exponential $J = J_0 \exp(T/T_0)$ dependence and a large value of $T_0 = 140$ K (measured between 120 K–200 K). The performance of this device (output power and threshold current density) is still significantly worst than our predictions and than the results from state of the art chirped superlattice lasers [4], [7], [8].

We do not yet have a good explanation for these low performance levels. Some indications are given however by a comparison between electroluminescence spectra taken from a LED [Fig. 5(a)] and subthreshold spectra of a laser device [Fig. 5(b)] processed from the same wafer (S1629). The electroluminescence spectra taken at 85 K for increasing currents in the LED device show the same characteristic transitions as in Fig. 3. The flat-band voltage (5.5 V), as indicated by the disappearance of the $6 \rightarrow 4$ transition, corresponds to the threshold voltage, showing that the amount of Be doping has been correctly designed. As expected, there is no Stark shift of the minigap transition that remains at a photon energy of 121 meV. In contrast, the amplified spontaneous emission spectra taken from the facet of the laser devices show a progressive red shift of the peak emission from $h\nu = 122$ meV to $h\nu = 118$ meV as the current is increased. This fairly large shift compared to the width of the luminescence line occurs as the applied voltage is changed by only a little more than a volt. Such a behavior can only be explained by assuming that the gain of the laser peaks at a lower energy than the fundamental transition. Thermal population of the lower miniband can be ruled out because this measurement was performed at low temperature (80 K) and the device still operated up to 200 K. A more likely explanation is the presence of a strong absorption peak at an energy close to the fundamental miniband transition, pushing the laser operation toward longer wavelengths. This absorption cannot be the normal waveguide losses due to free carriers since the latter would tend to increase with wavelength. A possibility is that the absorption originates from crystal imperfections or even nonoperating stages. Indeed, X-ray measurements show a lower crystalline material quality than the one obtained in our best devices.

ACKNOWLEDGMENT

The authors would like to thank T. Aellen for processing one of the samples used in this study.

REFERENCES

[1] J. Faist, F. Capasso, D. L. Sivco, C. Sirtori, A. L. Hutchinson, and A. Y. Cho, “Quantum cascade laser,” *Science*, vol. 264, p. 553, 1994.
[2] J. Faist, F. Capasso, C. Sirtori, D. L. Sivco, J. N. Baillargeon, A. L. Hutchinson, and A. Y. Cho, “High poer mid-infrared ($\lambda \sim 5$ μm) quantum cascade lasers operating above room temperature,” *Appl. Phys. Lett.*, vol. 68, p. 3680, 1996.
[3] C. Gmachl, A. Tredicucci, F. Capasso, A. L. Hutchinson, D. L. Sivco, J. N. Baillargeon, and A. Y. Cho, “High-power 8 μm quantum cascade lasers wity near optimum performance,” *Appl. Phys. Lett.*, vol. 72, p. 3130, 1998.
[4] S. Slivken, A. Matlis, A. Rybaltowski, Z. Wu, and M. Razeghi, “Low-threshold 7.3 μm quantum cascade lasers grown by gas-source molecular beam epitaxy,” *Appl. Phys. Lett.*, vol. 74, p. 2758, 1999.
[5] J. Faist, F. Capasso, C. Sirtori, D. L. Sivco, A. L. Hutchinson, S. N. G. Chu, and A. Y. Cho, “Short wavelength ($\lambda \sim 3.4$ μm) quantum cascade laser based on strain-compensated InGaAs/AllnAs,” *Appl. Phys. Lett.*, vol. 72, pp. 680–682, 1998.
[6] G. Scamarcio, F. Capasso, C. Sirtori, J. Faist, D. L. Sivco, A. L. Hutchinson, and A. Y. Cho, “High power infrared ($\lambda \sim 8$ μm) superlattice lasers,” *Science*, vol. 276, p. 773, 1997.
[7] A. Tredicucci, F. Capasso, C. Gmachl, D. L. Sivco, A. L. Hutchinson, A. Y. Cho, J. Faist, and G. Scamarcio, “High-power inter-miniband lasing in intrinsic superlattices,” *Appl. Phys. Lett.*, vol. 72, pp. 2388–2390, 1998.
[8] A. Tredicucci, F. Capasso, C. Gmachl, D. L. Sivco, A. L. Hutchinson, and A. Y. Cho, “High-power inter-miniband lasing with graded superlattices,” *Appl. Phys. Lett.*, vol. 73, pp. 2101–2103, 1998.
[9] J. Faist, A. Muller, and M. Beck, “Quantum cascade lasers based on superlattice active region and N-I-P-I doping,” in *Proc. 11th Int. Conf. Indium Phosphide and Related Compounds*, vol. 16, May 20, 1999, p. 11.
[10] A. Tredicucci, C. Gmachl, F. Capasso, D. L. Sivco, A. L. Hutchinson, and A. Y. Cho, “A Multiwavelength Semiconductor Laser,” *Nature*, vol. 396, p. 350, 1998.